Wind effects, unsteady behaviors, and regimes of propagation of surface fires in open field

Dominique Morvan

WIND EFFECTS, UNSTEADY BEHAVIORS, AND REGIMES OF PROPAGATION OF SURFACE FIRES IN OPEN FIELD

Dominique Morvan
Aix-Marseille Université, Laboratoire M2P2 UMR CNRS 7340, UNIMECA Technopôle de Château Gombert, Marseille, France

The subject of this article concerns the unsteady effects (fire intensity, wind) upon the prop-agation and, more generally, the behavior of surface fires in open fields. The study focused on two sources of unsteadiness: the first one resulting from the regime of propagation (wind driven or plume dominated), which can affect greatly the behavior of the flame front and con-sequently the fire intensity, the second one resulting from the wind gusts associated with the conditions of flow of wind in real conditions. The study was based on numerical simulations, using a multiphase formulation, and on spectral analysis of the time evolution of the fire line intensity. The calculations were performed in 2D for a homogeneous vegetation layer (grassland) and for a large interval of wind conditions (10 m open wind velocity U10 ranged between 1 m/sand 25m/s). The results have highlighted the link between the unsteady char-acter of flame front behavior and the regime of propagation (plume dominated, wind driven). A particular interest was focused on the role played by two potential sources of instabilities, namely the Kelvin-Helmholtz instability (wind effects) and the thermo-convective instability (plume effects), upon the behavior of fires. A second set of simulations has been carried out using unsteady wind conditions, reproduced using sinusoidal boundary conditions for the streamwise velocity, with a frequency ranging between 0.5 Hz and 3 Hz.

Keywords: Fire modeling; Unsteady phenomena; Wildfire behavior; Wind effects

INTRODUCTION

As formalized by Countryman (1972), the three factors affecting the most behavior of wildfires and forming the fire triangle are: weather, topography, and fuel (see also Pyne et al., 1996). With ambient temperature and relative air humidity, the wind intensity is a part of the weather conditions that affect significantly the conditions of ignition and propagation of wildfires (Benson, 2009). As underlined by Benson (2009), three kinds of "wind" can affect the behavior of wildfires: geostrophic wind resulting from the general meteorological conditions, local thermal wind resulting from a differential of temperature between sea and earth, and the wind induced by the fire itself under the action of the buoyancy. Many experimental studies carried out at small and large scale, through various vegetation layers (dead fuel beds, grasslands, shrublands) have highlighted a power law relationship between

Address correspondence to Dominique Morvan, UNIMECA, 60 rue Joliot Curie, Technopôle de Château Gombert, Marseille 13453 cedex 13, France. E-mail: dominique.morvan@univ-amu.fr

the rate of spread (*ROS*) of surface fires and the 2 m or 10 m open wind velocity ($U_W = U_2$ or U_{10}) (Catchpole et al., 1998; Fernandes, 2001; Fernandes et al., 2000; Rothermel and Anderson, 1966; Trabaud, 1979):

$$ROS = A \times U_W^B \tag{1}$$

with an exponent B, which can vary from 0.4 (Trabaud, 1979; in shrubland) to 2 (McArthur, 1966; in grassland). In grassland, experimental fires and wildfires observations (Fogarty and Alexander, 1999) have shown that the curve characterizing the relationship *ROS* versus U_W can be decomposed in three zones: a linear zone ($B \sim 1$) for wind speed ranged between 5.5 and 11 m/s, bounded by two nonlinear zones for weak ($U_W < 1$ m/s and $B > 1$) and strong ($U_W > 14$ m/s and $B < 1$) wind conditions. The same kind of behavior has been also observed for shrub land covers, from numerical simulations performed using a multiphase formulation (Morvan and Dupuy, 2004). At small scale, for experimental fires through solid fuel beds, the variations of this exponent have been related to the surface area volume ratio (Rothermel and Anderson, 1966). Exceeding relatively strong wind conditions, experimental data highlighted that the rate of variation of the curve *ROS* versus U_W changed and exhibited a decreasing part (McArthur, 1969; Rothermel, 1972). At large scale for surface fires in grasslands, Cheney et al. (1998) have showed that the linear relationship between *ROS* and U_W can be only observed until the wind speed velocity was less than 1.4 m/s; above this value, a power law relation has been observed characterized by an exponent $B < 1$ ($B \sim 0.84$). In the same paper, the authors suggested that this exponent must vary with the wind conditions. Pitts (1991), Cheney et al. (1998), and Morvan et al. (2013) reported the role played by the orientation of the wind vector compared to the direction of fire propagation (backing fire/heading fire transition). Sullivan (2007), Morvan and Dupuy (2004), and Morvan (2011) have underlined the importance of two regimes of propagation (wind driven and plume dominated) upon the effect of wind conditions on the propagation of surface fires. The transition between these two regimes of propagation has been very often analyzed, in introducing two non-dimensional numbers: the Froude number (*Fr*) and the Byram's convective number (*Nc*). These two physical parameters represent the ratio between two forces (expressed in module or in power), namely, the inertia of the wind and the buoyancy due to the thermal plume, governing the trajectory of the flame and consequently the heat transfer between the flame and the vegetation:

$$Fr = \frac{U_W^2}{gL_f} \qquad Nc = \frac{2gI_B}{\rho C_P T_0 (U_W - ROS)^3} \tag{2}$$

where g is the acceleration of gravitation; I_B and L_f are the fireline intensity and a flame length scale; ρ, C_P, and T_0 are the density, the specific heat, and the temperature of the ambient air; *ROS* is the fire rate of spread.

Experimental results obtained in a fire wind-tunnel (Beer, 1991) highlighted a sudden change of slope in the curve *ROS* versus U_W, which can be attributed to a change in the mode of energy transfer (by convection and radiation) between the flame and the solid fuel. Beer (1991) underlined the role played by vertical fluctuations of the wind flow upon the propagation of plume dominated fires.

Many phenomena affecting the coupling between wildfires and atmosphere are nonlinear; this characteristic is certainly at the origin of the difficulty in reducing the relationship between the fire rate of spread and the wind speed to a single power law function (Clark et al., 1999). As underlined in a recent article (Finney et al., 2012), we are far from fully answering the following question: "How does fire spread in dry grass, and why does it spread faster when the wind blows?" In the same paper, Finney has also underlined that the 3D structure of the flame front, characterized by the formation of vertical peaks and breaks, allowed the wind flow to cross the fire front, which affected significantly the fire dynamics and the fire/atmosphere interaction.

From the point of view of safety of people in charge of fire fighting or prescribed burning operations, the sudden modifications of fire behavior is as important as its average behavior. Infrared images of experimental crown fires (Coen, 2003) allowed in highlighting the existence of bursts of flame, characterized by velocity vectors with a module one order of magnitude larger than the local wind speed, which can affect significantly the fire front dynamics especially for a fire propagating along a slope terrain. Two experimental campaigns carried in grassland in Texas (Pilot Study in 2005, FireFlux in 2006) (Clements et al., 2008) have shown that turbulence (TKE) measured during the propagation of a fire can be four times larger than atmospheric turbulence (TKE) measured near the ground far from fire.

The behavior of fires driven by radiation heat transfers (such as plume dominated fires) is certainly more difficult to predict than fires driven by convective heat transfer (wind driven fires). The main reason of this difference of predictability is that, when we analyze the two terms representing these two mechanisms of heat transfer in the energy balance equation in the solid fuel, the first one (because of the Stefan-Boltzman σT^4 law) is much more nonlinear than the second one (which is more or less linear) (Morvan, 2011). For a long time the wind effects and consequently the wind driven fires have been considered to be the most critical conditions in terms of safety for structures and people potentially affected by this natural hazard. This is also the more convenient conditions (if the wind is not too strong) to conduct experimental fires. For all of these reasons, this regime of fire propagation is more known than the other one (plume dominated fires). Unfortunately, when the vegetation is very dry and characterized by a great accumulation of biomass, the power of the buoyant flow generated by the thermal plume can force the transition toward a plume dominated fire, which can also be catastrophic (such as the situation observed during the black Saturday in February 2009 in Australia) (Cruz et al., 2012).

From a simplified wind and flame configuration, Baines (1990) proposed an analysis on the relative importance of the two main mechanisms of heat transfer (by radiation and convection) governing the propagation of surface fires. The analysis was conducted in introducing a non-dimensional parameter P, representing the ratio between the heat flux received by the solid fuel by radiation and the convective cooling. Baines concluded rapidly that heat transfers between the flame and the vegetation were dominated at small scale by convection and at large scale by radiation. This conclusion is not fully confirmed by experimental observations carried out at large scale for crown fires (Clark et al., 1999; Stocks et al., 2004). The authors underline that at large scale the convective exchanges were enhanced by the turbulent flow and the radiation heat transfer increases because of the flame stretching.

The objective of this article was to study some unsteady behavior affecting the propagation of surface fires through a homogeneous vegetation layer (reproducing a tall grass) on a flat terrain. This problem has been studied using 2D numerical simulations. We know

that for strong enough wind conditions, wildfire fronts exhibit a 3D behavior, and appear as a more or less regular succession of peaks and troughs (Beer, 1991; Finney et al., 2013; Linn et al., 2012), which cannot be taken into account in 2D simulations. Unfortunately, 3D simulations need very large computing resources and, for this reason, some compromises must be introduced in the space resolutions (Linn et al., 2012), which can also limit the conclusions that can be extracted from these numerical simulations. For the same reasons, parametric studies are not always possible in 3D or remain always very expensive in terms of CPU time. A good compromise to study wildfires in 3D can be in using periodic boundary conditions along the vertical lateral boundaries, as it was proposed by Linn et al. (2012). Despite the limitations introduced in using a 2D approximation, this study must be considered as a first step in studying unsteady phenomena associated with wildfires behavior. This rough approach can highlight some general trends, for example, the character more or less predictable of some wildfire regimes (wind driven and plume dominated), and more generally the physical mechanisms associated with fires behavior. Of course, this analysis and the conclusions that we can extract from this simplified approach, must be refined in the future in performing 3D simulations.

This article was voluntarily limited to surface fires propagating on a flat terrain through a homogeneous vegetation layer. Heterogeneity of the vegetation and local variations of slope, which constitute also sources of uncertainties during the propagation of fire, have not been considered.

In the first part of the article, unsteady signals of fireline intensity have been analyzed for various steady average wind conditions (vertical logarithmic profile), ranged between 1 and 25 m/s. This relative large range of variations has allowed in covering the two regimes of fire propagation, namely, plume dominated and wind driven. Then the effect of a sinusoidal time variation of the wind flow has been explored for relatively moderated average wind conditions ($U_{10} = 2$ m/s, $\Delta U_{10} = \pm 1$ m/s), for frequencies ranging between 0.5 Hz and 3 Hz.

PHYSICAL AND MATHEMATICAL MODEL

The problem of the propagation of a surface fire through a vegetation layer has been simulated numerically using a multiphase formulation. This approach is similar to the model initially proposed by Grishin (1997), which has been extended with success to simulate in 2D and 3D various situations, such as surface fires in grassland (Morvan et al., 2009, 2013) and shrubland (Morvan and Dupuy, 2004), the efficiency of surface fuel reduction to prevent the vertical transition from surface to crown fire (Dupuy and Morvan, 2005), head fire/backfire interaction (Morvan et al., 2011, 2013), and the burning of a Douglas tree (Mell et al., 2009). The approach has been partially validated in comparing numerical results with experimental data obtained at small and large scale in various configurations (Mell et al., 2009; Morvan and Dupuy, 2001; Morvan et al., 2009, 2013).

In a few words, the model can be summarized as follows: The coupled system formed by the vegetation and the surrounding atmosphere has been represented as a sparse porous media (the vegetation) coupled with a gaseous phase (surrounding atmosphere, gaseous mixing coming from the pyrolysis and combustion processes). The various elements constituting the structure of the vegetation have been represented as a set of families of solid

fuel particles (foliage, twigs, trunk, etc.). The internal composition of each solid fuel element has been represented as a mixing of four components (water, dry matter, char, and ash), and each one was described using its own mass fraction. Assuming that the solid fuel elements of the vegetation stayed at rest, the evolution of the state of the vegetation (mass, volume, composition, temperature) was governed by a set of ordinary differential equations (ODE) representing the balance equations for mass and energy, and reproducing the different steps of degradation of the vegetation (drying, pyrolysis, and char combustion) resulting from the intense heating coming from the fire front. The degradation rates appearing on the right-hand side of these equations have been evaluated experimentally from thermal analysis of Mediterranean fuel samples and represented using an Arrhenius law process (pyrolysis and heterogeneous combustion) and threshold type process (drying).

The evolution of the gaseous phase is governed by the various physical mechanisms occurring inside the atmosphere surrounding the fire front: atmospheric turbulence and canopy turbulence interaction, mixing and combustion between gaseous pyrolysis products and ambient air, and radiation from the gas + soot mixture. Taking into account the important role played by the radiation heat transfer in the propagation of wildfires and considering the level of temperature fluctuations in the flame (see Morvan (2011) for the justifications), a particular effort has been done in this new version of the fire behavior model to simulate the turbulence/radiation interaction (TRI). Consequently, the radiation transfer equation (RTE) has been formulated using an optically thin fluctuation approximation (OTFA) (Coelho 2007; Siegel and Howell, 1992), as follows:

$$\begin{aligned}
&\frac{d\alpha_G \bar{I}}{\mathrm{ds}} = \alpha_G \left(\frac{\sigma \overline{\sigma_a T^4}}{\pi} - \overline{\sigma_a} \bar{I} \right) + \frac{\sigma_S \alpha_S}{4} \left(\frac{\sigma T_S^4}{\pi} - \bar{I} \right) \\
&\overline{\sigma_a T^4} \approx \overline{\sigma_a}\, \overline{T}^4 \left[1 + 6\frac{\overline{T'^2}}{\overline{T}^2} + 4\frac{\overline{\sigma_a' T'}}{\overline{\sigma_a}\,\overline{T}} \right] = \overline{\sigma_a}\overline{T}^4 \left[1 + 6\frac{\overline{T'^2}}{\overline{T}^2} + 4\frac{\overline{T'^2}}{\overline{\sigma_a}\,\overline{T}} \frac{\partial \sigma_a}{\partial T} \right] \\
&\frac{\partial \sigma_a}{\partial T} = 1862 \times \alpha_{soot}
\end{aligned} \tag{3}$$

The transport equation governing the temperature variance $\overline{T'^2} = \theta$ has been approximated as follows (Kenjeres et al., 2005):

$$\frac{\partial \bar{\rho}\theta}{\partial t} + \frac{\partial \bar{\rho}\tilde{u}_j\theta}{\partial x_j} = \frac{\partial}{\partial x_j}\left(\frac{\mu_{eff}}{\mathrm{Pr}_T} \frac{\partial \theta}{\partial x_j} \right) + 2P_\theta - 2\varepsilon_\theta \quad P_\theta = \frac{\mu_T}{\mathrm{Pr}_T}\left(\frac{\partial \overline{T}}{\partial x_j} \right)^2 \quad \varepsilon_\theta = \rho \frac{\theta}{2 \times R} \times \frac{\varepsilon}{K} \tag{4}$$

where, in agreement with experimental observations, the ratio between scalar and velocity dissipation time (R) has been assumed to be equal to 0.5 (Béguier et al., 1978).

We are conscious that the characteristics of flames for our problem, and especially the optical thickness defined as the product of the absorption coefficient by the turbulent integral length scale $\sigma_a \times l_t$, do not verify strictly the condition necessary for the use of the OTFA ($\sigma_a \times l_t << 1$) (Coehlo, 2007). A crude approximation of these two terms gives

an evaluation of the order of magnitude of optical thickness ranging between 1 and 5 (in assuming a temperature ranged between 1000 and 1500 K, a soot volume fraction ranged between 10^{-6} and 4×10^{-6}, and a turbulent integral length scale is equal to 0.5 m). From these values, we can conclude that the flames studied in this article can be considered as intermediate between thin and thick. However, one can consider that, despite this limitation, the use of the OTFA to simulate TRI constituted a progress in comparison to do nothing.

The numerical simulations were performed in a 2D domain: 170 m long by 35 m high. These dimensions were considered as sufficient to guarantee that the simulations reproduced correctly the propagation of a surface fire through a semi-infinite, 0.7 m depth fuel layer, without artificially forcing the behavior of the fire with open boundary conditions (at the top and at the outlet on the right end side). To control the direction of propagation of the fire, the fuel was fully removed within the first 20 m of the domain. Consequently, homogeneous fuel layer (0.7 m depth) was distributed between the position $X = 20$ m and $X = 170$ m (all of the fuel properties are reported in Table 1). Following the adaptive mesh refinement method described and validated in a previous study in 1D (Morvan and Larini, 2001) the mesh has been automatically refined in a region (20 m long) located on both sides of the fire front. The mesh size in this refined region has been chosen in following some physical considerations (Morvan, 2011), i.e., the grid size must be smaller than the extinction length scale and the depth of the vegetation layer. From these two constraints, the grid size along the two directions of the problem were fixed as follows: $\Delta_X = 0.25$ m, $\Delta_Z = 0.175$ m (see Table 1).

The physical properties characterizing the solid fuel layer were similar to the values collected on the field for a tall grass (fuel model #3 as described by Anderson (1982)). A 2-m-long gaseous burner (in injecting gaseous CO at 1600 K from the ground, with an injection velocity equal to 1 m/s) used to ignite the solid fuel layer, has been activated only 30 s after the beginning of the calculations (to be sure that the turbulent boundary layer flow was established before introducing the fire). In the absence of strong turbulence before that, the fire was fully developed; we cannot exclude that the combustion rate at the burner was partially piloted by the Arrhenius law and, consequently, the injected gaseous fuel must be hot enough to obtain a significant reaction rate. After having proceeded to some numerical tests, an arbitrary value of 1600 K has been chosen. Nevertheless, the properties characterizing the fire behavior (rate of spread, intensity, etc.) were evaluated after the fire had spread along a sufficient distance, to be sure to be not affected by these

Table 1 Solid fuel physical properties and external conditions imposed in the present numerical simulations

Solid fuel density (kg/m^3)	500
Volume fraction $\times 10^3$	2
Fuel moisture content (FMC) (%)	10
Fuel depth (m)	0.7
Fuel load (t/ha)	7
Surface area to volume ratio (m^{-1})	4000
Length of extinction (m)	0.5
Leaf Area Index (LAI)	2.8
10 m open wind velocity	1–25 m/s

Source: Anderson (1982); Burgan (1988).

ignition conditions. Preliminary numerical tests have also highlighted that an initialization time equal to 30 s was long enough to stabilize the turbulence boundary layer profile inside and above the vegetation layer. To facilitate the ignition of the fuel, the first 2 m were artificially dryed (FMC = 5%), once the ignition of the vegetation layer was confirmed, BS the burner was stopped. A logarithmic velocity profile has been imposed at the inlet of the computational domain (left-hand side) and as an initial condition for the velocity vectors field:

$$U_X(z) = A \times U_{10} \times Ln\left(\frac{z + z_0}{z_0}\right) \tag{5}$$

The constant A was adapted to fix the velocity magnitude 10 m above the ground level (10 m open wind velocity, i.e., U_x ($z = 10$ m) $= U_{10}$), in assuming a nude ground at the entrance of the domain, a value equal to $z_0 = 0.01$ m has been used for the roughness length z_0 in Eq. (5).

To quantify the behavior of fires, some global parameters have been extracted from numerical results, such as the rate of spread (ROS) evaluated from the first derivative of the time trajectory of the pyrolysis front, in assuming that this last one can be located by the isotherm in the solid fuel, $T_S = 500$ K temperature at which the rate of pyrolysis reaches its maximum value (Morvan and Dupuy, 2004; Pyne et al., 1996), the fireline intensity (in kW/m), and the Byram convective number, defined as follows:

$$I_B = \dot{m} \times \Delta H \qquad N_C = \frac{2gI_B}{\rho C_P T_0 \left(U_{10} - ROS\right)^3} \tag{6}$$

where $\dot{m}$ is the mass loss rate (only the dry fuel, in kg/m.s), $\Delta H = 18{,}000$ kJ/kg designates the heat of combustion (Burgan, 1988; Pyne et al., 1996), g is the acceleration of gravity, ρ is the air density (standard conditions), T_0 and C_P are the temperature and the specific heat of ambient air.

Moreover, the propagation of the fire front reached rapidly a quasi steady state, and all the trajectories of the solid fuel temperature were parallel. Consequently, the fact of choosing a particular value to evaluate the ROS did not affect the results.

UNSTEADY BEHAVIOR OF A SURFACE FIRE SUBMITTED TO A STEADY WIND FLOW

A first set of numerical simulations, under steady wind conditions has been performed, using a wind speed ranged between 1 and 25 m/s. This large domain of variation for this input parameter, allowed in covering the two regimes of propagations identified for surface fires, namely, the plume dominated fires and the wind driven fires. A first illustration of the temperature field (gaseous phase) obtained for three values of the wind speed ($U_{10} = 1$, 8, and 20 m/s) can be seen in Figure 1. This figure illustrates perfectly one of the consequences resulting from the balance between the two forces governing the behavior of the fire, namely, the inertia of the wind and the buoyancy from the difference of temperature (and consequently the density) between the plume and the ambient air. As the wind speed increased, the trajectory of the plume was more and more affected by this external

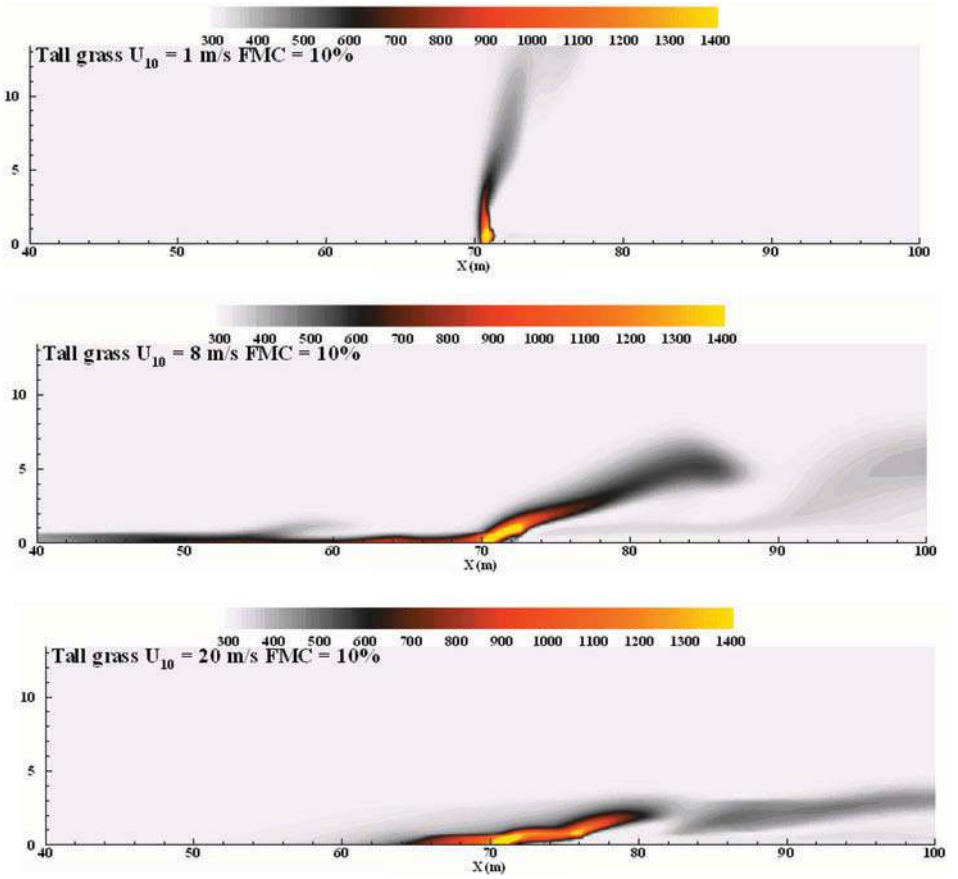

Figure 1 Temperature field calculated during the propagation of a surface fire for three wind flow conditions: $U_{10} = 1$ m/s, 8 m/s, and 20 m/s (top to bottom).

forcing and was more and more tilted toward the unburned vegetation. From a more general point of view, one of the parameters characterizing the behavior of the fire, the ratio between the rate of spread and the 10 m open wind velocity (ROS/U_{10}), can be expressed as a function the inverse of the convective Byram number ($1/N_C$) (see Eq. (2) and Figure 2). With the values imposed for the wind speed and those obtained for the *ROS* and the fireline intensity, the resulting range of variation for $1/N_C$ was included between 7×10^{-4} to 10, which covered a large range of situations, from plume dominated fire ($1/N_C << 1$) to wind driven fire ($1/N_C >> 1$). The numerical results shown in Figure 2 highlight clearly that the maximum value of the ratio ROS/U_{10} was obtained for the smallest value of the parameter $1/N_C$. Due to quite low fuel moisture content conditions, the *ROS* can represent 46% of the 10 m open wind speed. Experimental observations for grassland fires in Australia reported by Cheney et al. (1998) have shown values larger than 50%. The same curve has shown also that for larger values of $1/N_C$ (>>1)1), the ratio ROS/U_{10} converged more or less toward a constant value (around 8%), revealing a nearly linear relationship between *ROS* and U_{10}. Variations of the fire behaviors can also be highlighted for the time variations of the fireline intensity, both the average value $<I_B>$(Figure 3) and the standard

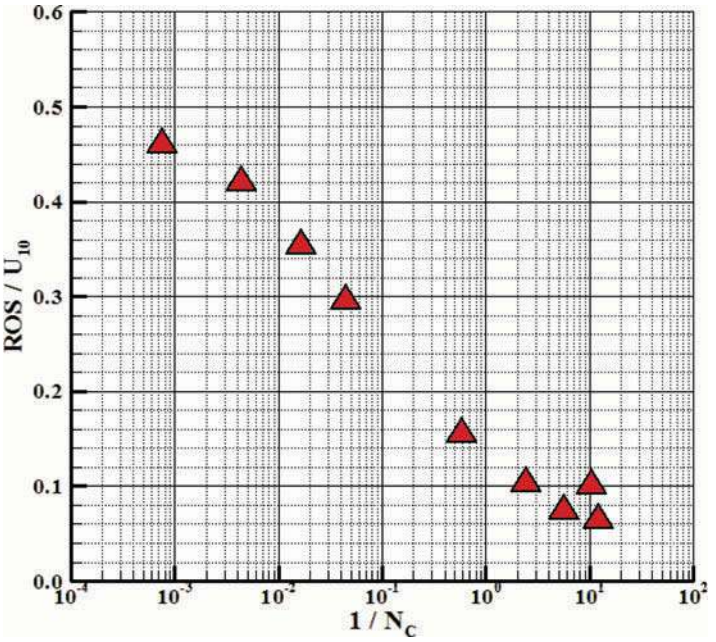

Figure 2 Ratio fire rate of spread/wind speed (ROS/U_{10}) as a function of the convective Byram number.

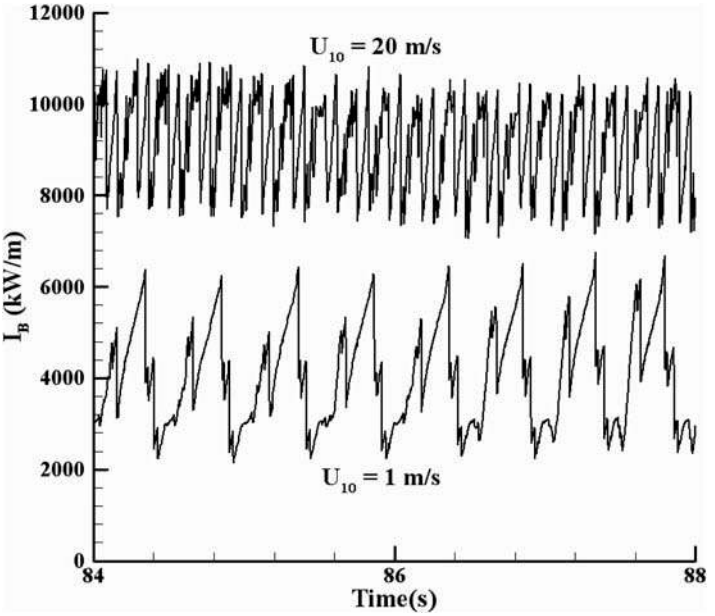

Figure 3 Time history of the fireline intensity for two wind conditions ($U_{10} = 1$ and 20 m/s).

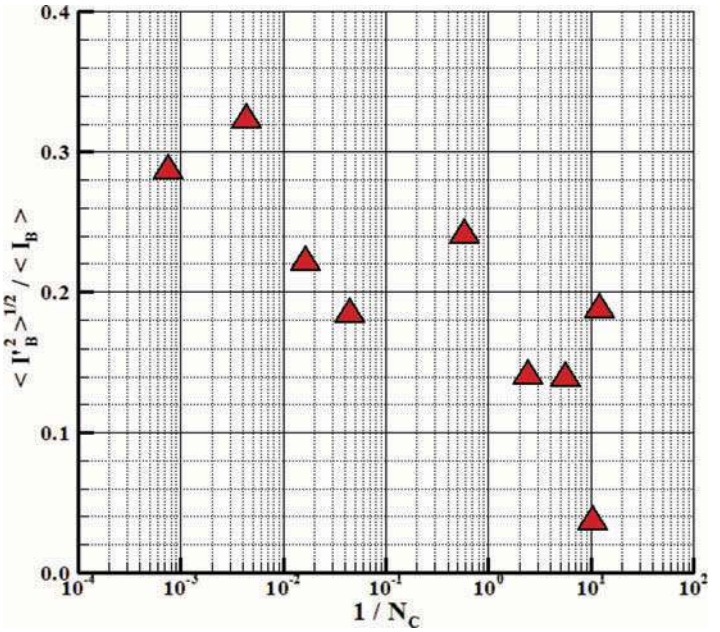

Figure 4 Ratio standard deviation/mean value for the fireline intensity as a function of the convective Byram number.

deviation $<I_B{}'^2>^{1/2}$ (Figure 4). The two curves in Figure 3 and representing the time evolution of the fireline intensity signal obtained for two values of the 10 m open wind speed (U_{10}) show clearly a great modification of the dynamic of the fire in terms of amplitude and frequency of the fire intensity signal. The general trend shown for the curves representing standard deviation, normalized using the average value, versus the inverse convective Byram number (Figure 4), can be summarized as follows: for plume dominated fires ($1/N_C << 1$) the fire front exhibited (in relative values) larger fluctuations than for wind driven fires ($1/N_C >> 1$). As indicated in the introduction, this feature (plus the impact upon the ratio ROS/U_{10}) increases the character more unpredictable of plume dominated fires. This particularity can certainly be attributed to the increase of nonlinear mechanisms (such as radiation) governing the heat transfers between the fire front and the vegetation.

As indicated in the introduction, two forces, namely, the inertia of the wind and the buoyancy due to the difference of temperature between the plume and the ambient atmosphere, can affect the trajectory of the flame and consequently the behavior of fires. Therefore, two mechanisms of instability (associated to these two forces) can be associated to the unsteady behavior of the fire: the Kelvin-Helmholtz instability resulting from the shearing between the wind and the vegetation and the thermo-convective instability resulting from the difference of density between the plume and the ambient air.

The Strouhal number (obtained experimentally) associated with the Kelvin–Helmholtz instability (characterized by a frequency F_{KH}) above a canopy (longitudinal mode) (Kaimal and Finnigan, 1994) defined using the wind velocity at the top of the canopy (U_H) is equal to 0.15, taking into account that for a logarithmic wind profile, $U_H = 0.62 \times U_{10}$ (U_{10}: 10 m open wind velocity), the Strouhal number defined using this reference wind velocity can be written as:

$$S_t = \frac{F_{KH} \times H}{U_{10}} = 0.15 \times 0.62 = 0.093 \tag{7}$$

The characteristic frequency (F_B) associated with the puffing instability of the fire plume can be evaluated using the same expression highlighted for a pool fire (Cox, 1995; Hamins et al., 1996) (g = acceleration of gravitation):

$$F_B = (0.5 \pm 0.04) \left(\frac{g}{D_{Fire}} \right)^{1/2} \tag{8}$$

In this expression, the fire depth (D_{Fire}) has been evaluated as the product of the fire residence time by the rate of spread (ROS) (Morvan, 2013). As detailed in a previous publication (Morvan, 2013), the fire residence time was determined from the time history of the gas temperature recorded 0.25 m above the ground level. Compared to an evaluation of this quantity at the ground level, the main advantage of this procedure is to separate clearly the gas heating coming from the flaming combustion from the part in contact with the hot embers. A consequence of that is that the values found using this method are a little bit smaller than some common values reported in the literature.

To fix some typical values, for $H = 0.7$ m, $U_{10} = 2$ m/s and 20 m/s, we obtain the set of values shown in Table 2.

In order to clarify the role played by these two mechanisms of instability upon the fire dynamics, a spectral analysis (FFT) has been carried out on the fire intensity signal (time variations), in selecting an interval of time for which the fire had reached a quasi-steady behavior (see Figure 5). The Strouhal number formed using two sets of reference scales (related to inertial and buoyancy forces) versus the inverse of the convective Byram number has been reported in Figures 6 and 7. The two major conclusions that we can extract from these two curves are:

- When the frequency is reduced using the inertial scales, for large values of $1/N_C$ the corresponding Strouhal number converged toward a value nearly equal to 0.093.
- When the frequency is reduced using the buoyancy scales, for small values of $1/N_C$ the corresponding Strouhal number converged toward a value nearly equal to 0.5.

As indicated previously these two domains of variation of the convective Byram number (N_C), corresponds to wind driven and plume dominated fires, respectively. These results confirm the concept developed previously concerning the behavior of fires, in including also the unsteady part, i.e., wind driven fires are piloted by shear interactions between the wind

Table 2 Characteristics frequency of Kelvin–Helmholtz (F_{KH}), buoyant plume (F_B) instabilities, and fundamental mode (f) extracted from a FFT analysis of the fireline intensity signal for two values of the wind speed $U_{10} = 2$ and 20 m/s

U_{10} (m/s)	F_{KH} (Hz)	F_B (Hz)	f (Hz)
2	0.26	1.3	3.4
20	2.66	0.66	5.5

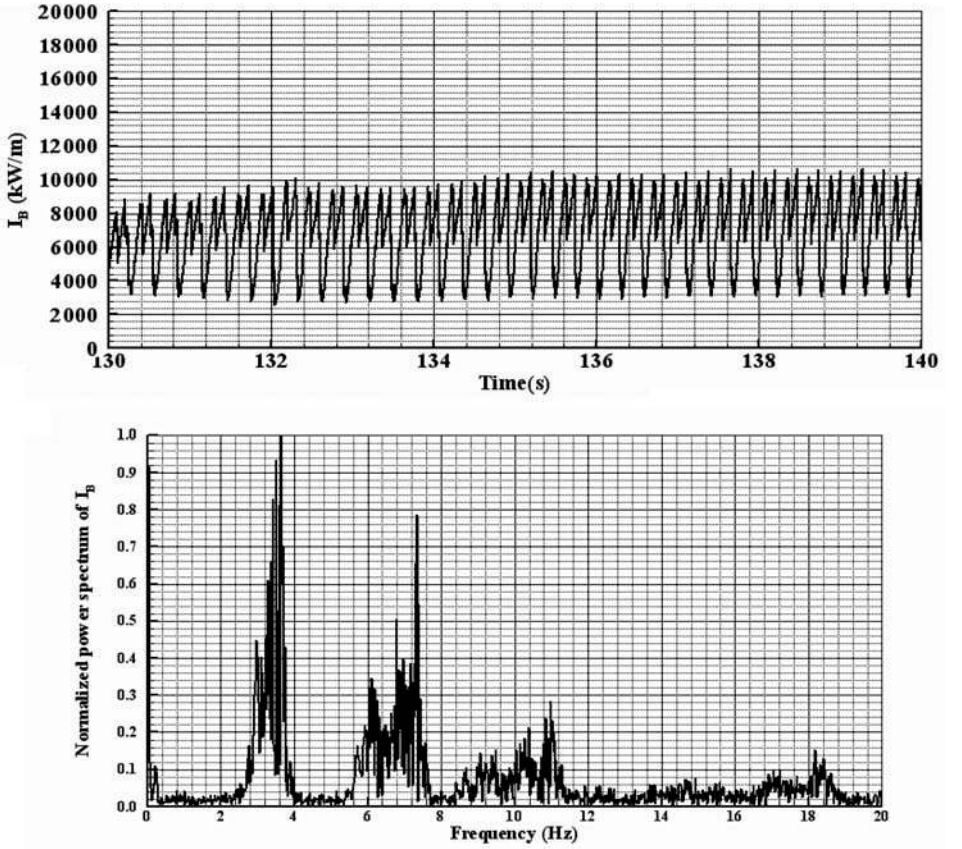

Figure 5 Time evolution (top) and FFT analysis of fireline intensity signal ($U_{10} = 2$ m/s).

flow and the canopy, whereas plume dominated fires are governed by thermo-convective instabilities between the plume and the ambient atmosphere.

The trend highlighted in Figure 6 for wind driven fires shows that the frequency characterizing the fire intensity signal increases when the wind speed increases. In the same manner, for plume dominated fires, the results shown in Figure 7 show that the same frequency must decrease if the depth of the vegetation layer increases. These results are in agreement with experimental results reported by Finney et al. (2013). The spectral analysis of temperature signals collected in these experiments had shown that the curve Strouhal number versus Froude number, did not match perfectly those observed for pool fire. Consequently, one can deduce from this observation (confirmed in the present numerical study) that for the great majority of situations the behavior of fires was governed under the combined action of two forces, namely, the inertia (wind) and the buoyancy (plume), and not from the action of a single one (except in extreme situations, very weak and very strong wind conditions). The shear flow resulting from the interaction of the wind flow with the vegetation, promoted the development of Kelvin–Helmholtz instability. Then the buoyancy resulting from the gradient of temperature between the thermal plume and the ambient atmosphere induced a lift effect in deviating these structures vertically (Finney et al., 2013).

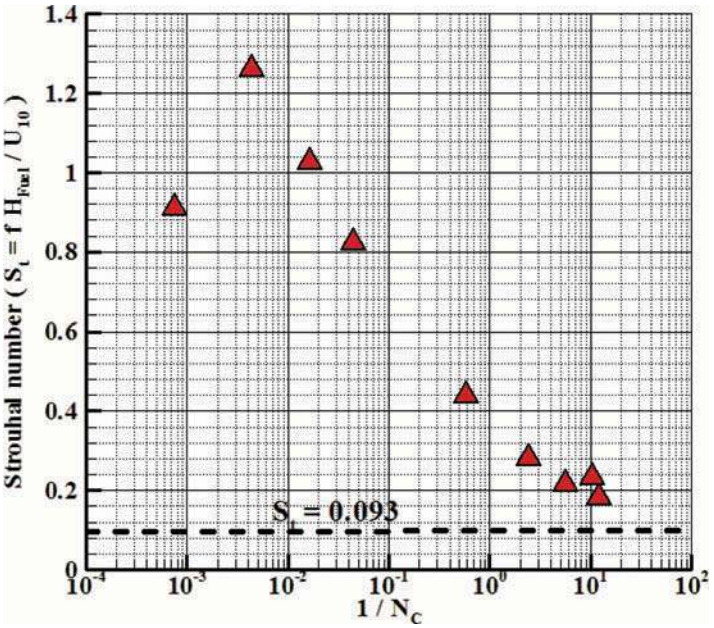

Figure 6 Evolution of the Strouhal number (inertial scales) as a function of the convective Byram number.

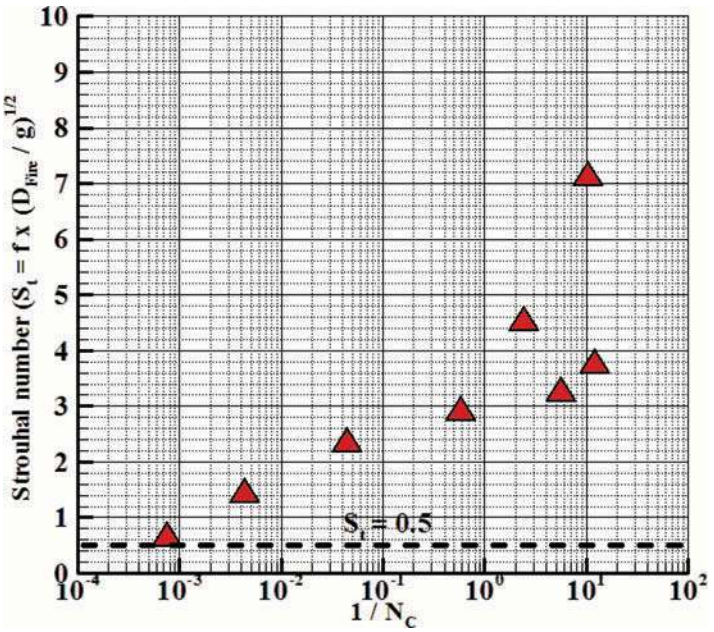

Figure 7 Evolution of the buoyant Strouhal number (plume scales) as a function of the convective Byram number.

UNSTEADY RESPONSE OF A SURFACE FIRE SUBMITTED TO AN UNSTEADY WIND FLOW

In order to study the response of the coupled system formed by the fire, the vegetation and the ambient air, to a time variation of wind conditions reproducing wind gusts, we have introduced at the inlet boundary a sinusoidal variation of the wind module, as follows:

$$U_X(z) = A \times U_{10} \times Ln\left(\frac{z+z_0}{z_0}\right) + \Delta U_{10} \sin(2\pi \times F \times t) \tag{9}$$

where ΔU_{10} and F designate, respectively, the amplitude and the frequency of wind variations. The present study has been limited to one wind conditions, $U_{10} = 2$ m/s and $\Delta U_{10} = 1$ m/s; the frequency F varied between 0.5 and 3 Hz. This wind condition ($U_{10} = 2$ m/s) has been chosen because it represents a situation for which we have found (in quasi steady wind conditions) a relatively high value of the variation of the rate of spread (ROS) versus U_{10} $\left(\frac{dROS}{dU_{10}}\right)$ (see Table 3).

As stated previously, the characteristic frequencies associated to this wind condition were: $F_{KH} = 0.26$ Hz (Kelvin-Helmholtz instability) and $F_B = 1.3$ Hz (Thermo-convective instability) (see Table 2).

In Figures 8 and 9, snapshots of the temperature field (gaseous phase) are shown at three different times and for two values of the wind gusts frequency ($F = 1$ and 0.5 Hz). As shown on these figures (the snapshot were taken exactly at the same time for the two frequencies), the trajectory of the fire front seemed to be not too much affected by the frequency of variations of the inlet wind flow. However, for $F = 0.5$ Hz (Figure 9), the vertical dynamics of the flame (part located above the vegetation top) was significantly affected and subjected to long wave (low frequency) oscillations, which were not observed for $F = 1$ Hz (Figure 8). The amplitude of variations of the inlet wind speed was ranged between 1 and 3 m/s, we have consequently reported in Figure 10 the trajectory of the pyrolysis front (isotherm $T_S = 500$ K in the solid phase) obtained for steady and unsteady ($F = 0.5$ and 1 Hz) state conditions. For comparison, we have also plot on the same curve the trajectory obtained (in steady state conditions) for $U_{10} = 1$ and 3 m/s. This figure shows that in terms of propagation, for these average wind conditions ($<U_{10}> = 2$ m/s), the fire behavior was not much affected by the unsteady character of the inlet wind conditions. Even if the result obtained for $F = 0.5$ Hz shows a small acceleration of the fire front at the end of the simulation, the trajectories of the fire front obtained in unsteady conditions did not differ significantly from one obtained in fully steady conditions (see Figure 10). The fire intensity signals obtained for these two conditions were far from similar (see Figure 11). While the signal for $F = 1$ Hz was nearly identical with the one obtained for a steady wind in exhibiting a peak of energy at 3.65 Hz (nearly equal to 3.4 Hz observed in steady conditions), whereas the signal obtained for $F = 0.5$ Hz was characterized by a peak of energy at 0.24 Hz (nearly equal to the frequency, $F_{KH} = 0.26$ Hz,

Table 3 Rate of spread (ROS) obtained for average wind conditions (U_{10}) ranged between 1 and 25 m/s

U_{10} (m/s)	1	2	3	4	8	12	15	20	25
ROS (m/s)	0.46	0.84	1.06	1.18	1.24	1.23	1.10	1.28	2.51

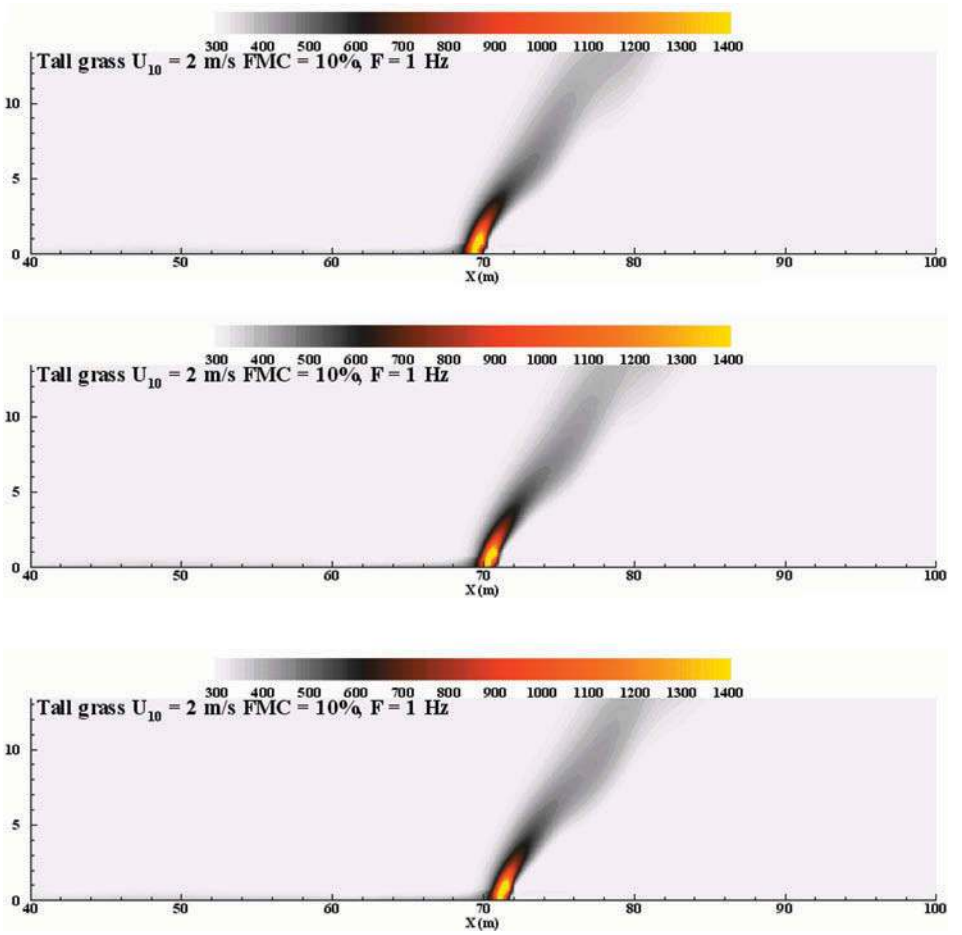

Figure 8 Snapshots of the temperature field (62, 63, and 64 s after the ignition) calculated for a surface fire propagating through a grassland under unsteady wind conditions ($U_{10} = <U_{10}>[1 + 0.5 \times \sin(2\pi Ft)]$, $<U_{10}>=$ 2 m/s, $F = 1$ Hz).

of the Kelvin-Helmholtz instability along the streamwise direction). This result suggests that even if the heat transfer between the flame and the vegetation was naturally responsible of the fire behavior, for these wind conditions ($<U_{10}> = 2$ m/s), the part of the flame situated above the top of the canopy (more affected by wind variations) must play a less important role upon the fire propagation than the part situated below the top of the canopy.

These results suggest in the following remarks:

- The variations of wind conditions affect mainly the part of the flame located above the top of the vegetation layer.
- The ROS of plume dominated fires is mostly affected by the part of the flame located below the top of the vegetation, which was evidently much less affected by wind variations.

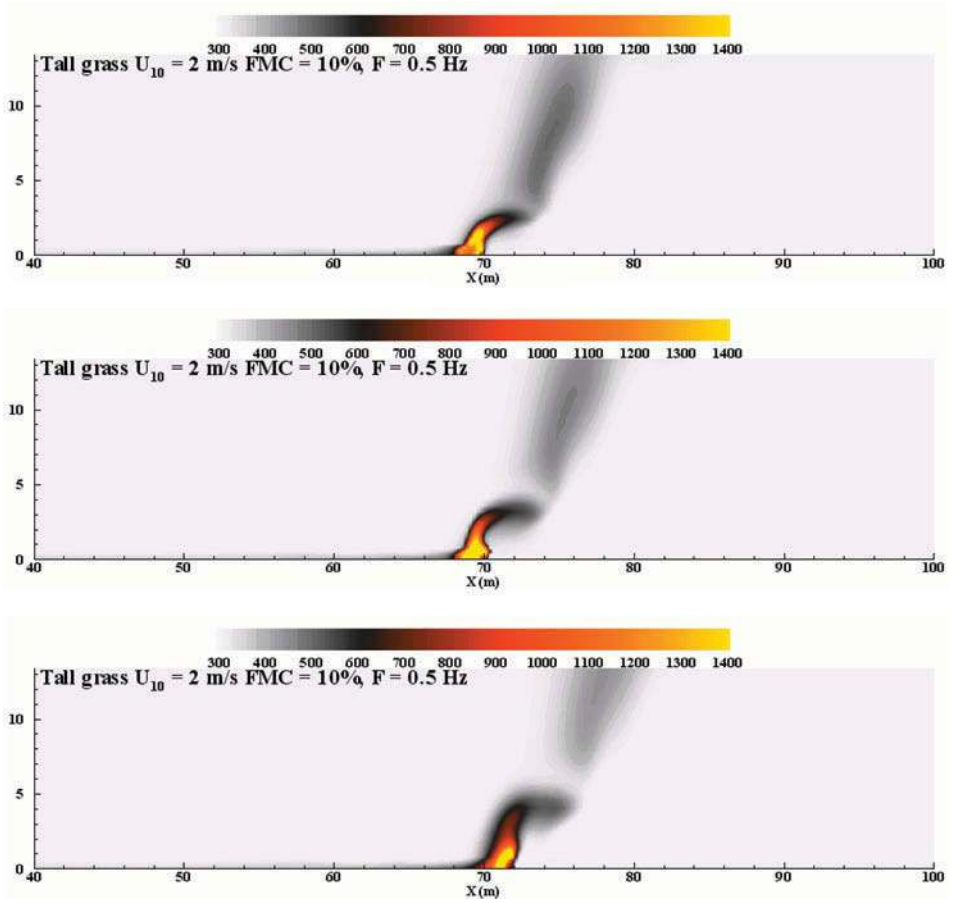

Figure 9 Snapshots of the temperature field (62, 63, and 64 s after the ignition) calculated for a surface fire propagating through a grassland under unsteady wind conditions ($U_{10} = <U_{10}>[1 + 0.5 \times \sin(2\pi Ft)]$, $<U_{10}>=$ 2 m/s, $F = 0.5$ Hz).

- One of the actions of wind gusts was to stimulate the mode associated with the Kelvin–Helmholtz instability (longitudinal mode).

This last remark has been confirmed in regarding the curve representing the evolution of the standard deviation of the fire intensity (normalized by the average fire intensity) versus the ratio F/F_{KH} (see Figure 12). This figure highlights clearly that in exciting the inlet wind flow with a frequency two times larger than the Kelvin-Helmholtz frequency ($F/F_{KH} = 2$), it can produce an increase by a factor 2 (in relative value) of the fluctuations of fire intensity. This factor 2 comes certainly from the fact that we have compared unsteady wind conditions with empirical results obtained for a steady flow configuration (with the additional possibility that the boundary condition imposed at the inlet flow, allowed the fire front to modify by aspiration the inlet flow). However, the result obtained for 0.25 Hz (F/F_{KH} nearly equal to 1) shows without any doubt that the maximal relative response was obtained for a ratio F/F_{KH} equal to 2 and not 1 as one could expected.

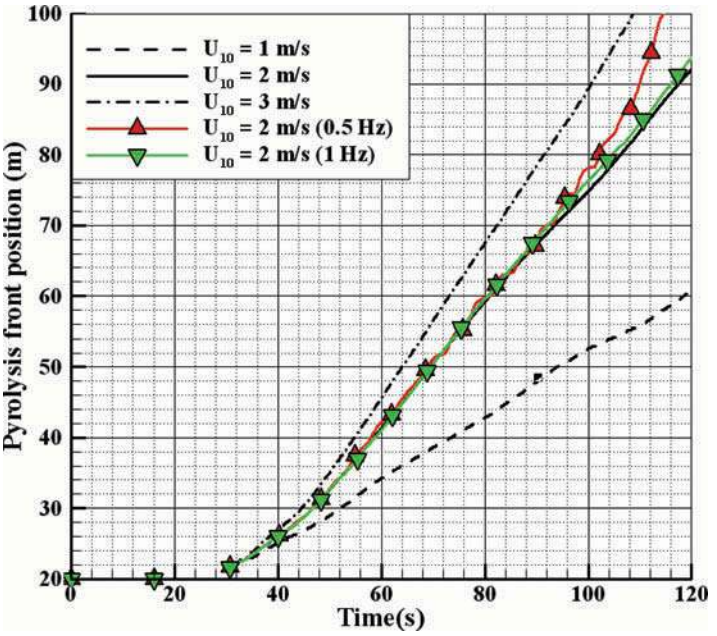

Figure 10 Time evolution of pyrolysis front ($T_S = 500$ K) calculated for various wind conditions (steady: U_{10} = 1, 2, and 3 m/s; unsteady: $<U_{10}>$= 2 m/s, $<\Delta U_{10}>$ = 1 m/s, ($F = 0.5$ and 1 Hz)).

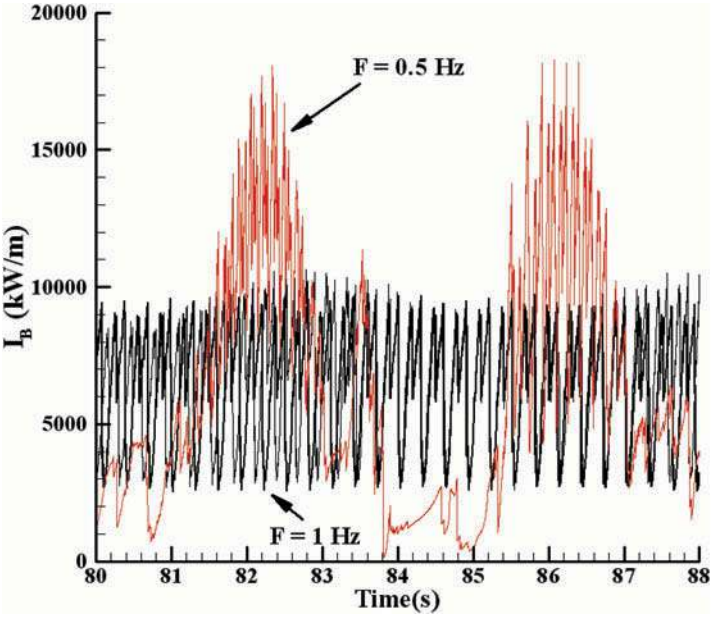

Figure 11 Time evolution of the fireline intensity calculated for two sinusoidal wind speed variations (F = 0.5 Hz and $F = 1$ Hz).

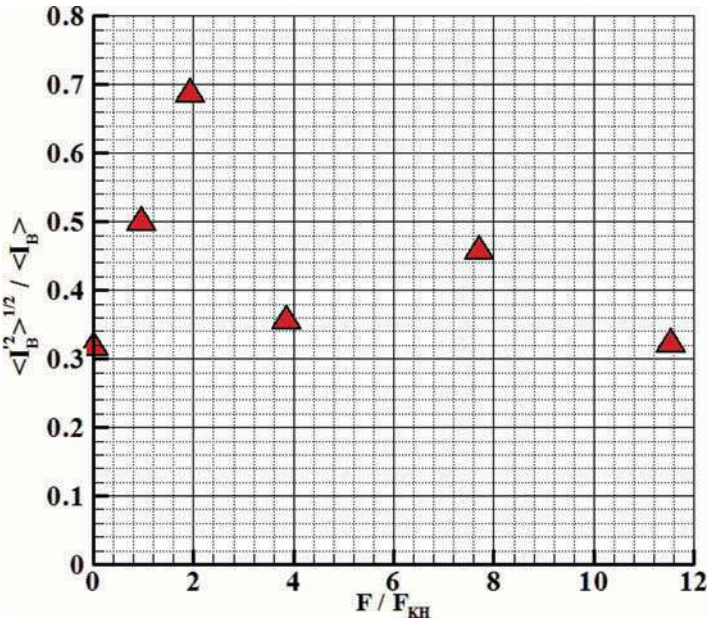

Figure 12 Reduced value of the fireline intensity standard deviation versus reduced wind gusts frequency ($<U_{10}>= 2$ m/s).

CONCLUSION

A set of numerical simulations reproducing the propagation of a surface fire on a flat terrain and through a homogeneous vegetation layer has been performed to identify some phenomena characterizing the behavior of fire in various regimes of propagation, from plume dominated fires to wind driven fires. The analysis of the results concerning the time evolution of the fire intensity has shown that plume dominated fires were subject to larger time variations than wind driven fires, with a consequence that the behavior of this kind of fire was much more difficult to predict that the other one. In terms of frequencies, wind driven fires were clearly dominated by shear effects (Kelvin–Helmholtz instability) and plume dominated fires were driven by thermo-convective instability. Preliminary results obtained for weak wind conditions have highlighted that a maximum impact (in terms of unsteadiness) can be obtained if the inlet wind intensity was excited in using a frequency two times larger than the frequency characterizing the Kelvin-Helmholtz (streamwise mode) instability associated with the shear interaction between the wind flow and the canopy.

ACKNOWLEDGMENT

The author wishes to thank the anonymous reviewers for their constructive remarks and the detailed analysis of the article, which allowed us to clarify some points and to improve significantly the presentation of this study.

FUNDING

This study was supported by the Agence Nationale de la Recherche (Project No.: ANR-09-COSI-006).

REFERENCES

Anderson, H.E. 1982. Aids to determining fuel models for estimating fire behaviour. Gen. Tech. Rep. INT-122. USDA-FS, Intermountain Research Station, Ogden, UT.

Baines, P.G. 1990. Physical mechanisms for the propagation of surface fires. *Math. Comput. Modell.*, **13**(2), 83–94.

Beer, T. 1991. The interaction of wind and fire. *Boundary Layer Meteorol.*, **54**, 287–308.

Béguier, C., Dekeyser, I., and Launder, B.E. 1978. Ratio of scalar and velocity dissipation time scales in shear flow turbulence. *Phys. Fluids*, **21**(3), 307–310.

Benson, R.P. 2009. Climatic and weather factors affecting fire occurrence and behaviour. In *Developments in Environmental Science*, vol. 8. Bytnerowicz, A., Arbaugh, M., Riebau, A., and Andersen, C. (Eds.), Elsevier, Amsterdam, pp. 37–59.

Burgan, R.E. 1988. Revisions to the 1978 National Fire-Danger Rating System. Res. Pap. SE-273. USDA-FS, Asheville, NC.

Catchpole, W.R., Catchpole, E.A., Butler, B.W., Rothermel, R.C., Morris, G.A., and Latham, D.J. 1998. Rate of spread of free-burning fires in woody fuels in a wind tunnel. *Combust. Sci. Technol.*, **131**, 1–37.

Cheney, N.P., Gould, J.S., and Catchpole, W.R. 1998. Prediction of fire spread in grasslands. *Int. J. Wildl. Fire*, **8**(1), 1–13.

Clark, T.L., Radke, L., Coen, J., and Middleton, D. 1999. Analysis of small-scale convective dynamics in a crown fire using infrared video camera imagery. *J. Appl. Meteorol.*, **38**, 1401–1420.

Clements, C.B., Zhong, S., Bian, X., Heilman, W.E., and Byun, D.W. 2008. First observations of turbulence generated by grass fires. *J. Geophys. Res. D: Atmos.*, **113**, 13.

Coelho, P.J. 2007. Numerical simulation of the interaction between turbulence and radiation in reactive flow. *Prog. Energy Combust. Sci.*, **33**, 311–383.

Coen, J.L. 2003. Infrared imagery applied into wildland fire dynamics. Presented at the 5th Symposium on Fire and Forest Meteorology, Orlando, Florida, November 16–20.

Countryman, C.M. 1972. The fire environment concept. Pacific Southwest Forest and Range Experiment Station, US Forest Service.

Cox, G. 1995. *Combustion Fundamentals of Fire*, Academic Press, London.

Cruz, M.G., Sullivan, A.L., and Gould, J.S. 2012. Anatomy of a catastrophic wildfire: The black Saturday Kilmore east fire in Victoria, Australia. *Forest Ecol. & Manage.*, **284**, 269–285.

Dupuy, J.L., and Morvan, D. 2005. Physical modelling of forest fire behaviour in a fuel break. *Int. J. Wildland Fire*, **14**, 141–151.

Fernandes, P.A.M. 2001. Fire spread prediction in shrub fuels in Portugal. *For. Ecol. Manage.*, 144, 67–74.

Fernandes, P.A.M., Catchpole, W.R., and Rego, F.C. 2000. Shrubland fire behaviour modelling with microplot data. *Can. J. For. Res.*, **30**, 889–899.

Finney, M.A., Cohen, J.D., McAllister, S.S., and Jolly, W.M. 2012. On the need for a theory of wildland fire spread. *J. Wildl. Fire* (special issue), **22**(1), 25–36.

Finney, M.A., Forthofer, J., Grenfell, I.C., Adam, B.A., Akafuah, N.K., and Saito, K. 2013. A study of flame spread in engineering cardboard fuelbeds. Part I: Correlations and observations. Presented at the 7th International Symposium on Scale Modeling (ISSM-7), Hirosaki, Japan, August 6–9.

Fogarty, L.G., and Alexander, M.E. 1999. A field guide for predicting grassland fire potential. *Fire Technol. Trans. Note*, **20**, 10.

Grishin, A.M. 1997. *Mathematical Modelling of Forest Fires and New Methods of Fighting Them*. Albini, F. (Ed.). Tomsk State University, Tomsk, Russia, p. 367.

Hamins, A., Kashiwagi, T., and Burch, R.R. 1996. Characteristics of pool fire burning. ASTM STP 1284.

Kaimal, J.C., and Finnigan, J.J. 1994. *Atmospheric Boundary Layer Flows*, Oxford University Press, Oxford, UK.

Kenjeres, S., Gunarjo, S.B., and Hanjalic, K. 2005. Contribution to elliptic relaxation modeling of turbulent natural and mixed convection. *Int. J. Heat Fluid Flow*, **26**, 569–586.

Linn, R.R., Canfield, J.M., Cunningham, P., Edminster, C., Dupuy, J.L., and Pimont, F. 2012. Using periodic line fires to gain a new perspective on multi-dimensional aspects of forward fire spread. *Agric. For. Meteorol*., **157**, 60–76.

McArthur, A.G. 1966. *Weather and Grassland Fire Behaviour*, Forest Research Institute, Forestry and Timber Bureau, ACT, Australia.

McArthur, A.G. 1969. The Tasmanian Bushfire of 7th February 1967, and Associated Fire Behaviour Characteristics, vol. 1, Technical Co-operation Programme, Mass Fire Symposium (Canberra, Australia 1969), Maribyrnong, Victoria, Defence Standards Laboratories.

Mell, W., Maranghides, A., McDermott, R., and Manzello, S. 2009. Numerical simulation and experiments of burning Douglas fir trees. *Combust. Flame*, **156**, 2023–2041.

Morvan, D. 2011. Physical phenomena and length scales governing the behaviour of wildfires: A case for physical modelling. *Fire Technol*., **47**, 437–460.

Morvan, D. 2013. Numerical study of the effect of fuel moisture content (FMC) upon the propagation of a surface fire on a flat terrain. *Fire Saf. J*., **58**, 121–131.

Morvan, D., and Dupuy, J.L. 2001. Modeling of fire spread through a forest fuel bed using a multiphase formulation. *Combust. Flame*, **127**, 1981–1994.

Morvan, D., and Dupuy, J.L. 2004. Modeling the propagation of a wildfire through a Mediterranean shrub using a multiphase formulation. *Combust. Flame*, **138**, 199–210.

Morvan, D., Hoffman, Ch., Rego, F., and Mell, W. 2011. Numerical simulation of the interaction between two fire fronts in grassland and shrubland. *Fire Saf. J*., **46**, 469–479.

Morvan, D., and Larini, M. 2001. Modeling of one dimensional fire spread in pine needles with opposing air flow. *Combust. Sci. Technol*., **164**, 37–64.

Morvan, D., Meradji, S., and Accary, G. 2009. Physical modelling of fire spread in grasslands. *Fire Saf. J*., **44**, 50–61.

Morvan, D., Meradji, S., and Mell, W. 2013. Interaction between head fire and backfire in grasslands. *Fire Saf. J*., **58**, 195–203.

Pitts, W.M. 1991. Wind effects on fires. *Prog. Energy Combust. Sci*., **17**, 83–134.

Pyne, S.J., Andrews, P.L., and Laven, R.D. 1996. *Introduction to Wildland Fire*, 2nd ed., John Wiley & Sons, New York.

Rothermel, R.C. 1972. A mathematical model for predicting fire spread in wildland fuels. USDA Forest Service RP INT-115.

Rothermel, R.C., and Anderson, H.E. 1966. Fire spread characteristics determined in the laboratory. USDA Forest Service RP INT-30.

Siegel, R., and Howell, J.R. 1992. *Thermal Radiation Heat Transfer*, 3rd ed. Hemisphere Publishing Corporation, Washington.

Stocks, B.J., Alexander, M.E., and Lanoville, R.A. 2004. Overview of the International Crown Fire Modelling Experiment (ICFME). *Can. J. For. Res*., **34**, 1543–1547.

Sullivan, A.L. 2007. Convective Froude number and Byram's energy criterion of Australian experimental grassland fires. *Proc. Combust. Inst*., **31**, 2557–2564.

Trabaud, L. 1979. Etude du comportement du feu dans la garrigue de chêne kermes à partir des températures et des vitesses de propagation. *Ann. Sci. For*., **36**, 13–35.